2021 IEEE/RSJ International Conference on Intelligent Robots and Systems (IROS)
September 27 - October 1, 2021. Prague, Czech Republic

2021 IEEE/RSJ International Conference on Intelligent Robots and Systems (IROS) | 978-1-6654-1714-3/21/$31.00 ©2021 IEEE | DOI: 10.1109/IROS51168.2021.9636735

# Wing Fold and Twist Greatly Improves Flight Efficiency for Bat-Scale Flapping Wing Robots

Xiaozhou Fan[1], Kenneth Breuer[2] and Hamid Vejdani[3]

***Abstract*— Inspired by bat flight performance, we explore the advantages of wing twist and fold for flapping wing robots. For this purpose, we develop a dynamical model that incorporates these two degrees of freedom to the wing. The twist is assumed to be linearly-increasing along the wing, while the wing fold is modeled as a relative rotation of the handwing with respect to the armwing. An optimization scheme parameterizes the wing kinematics for 2, 5 and 8 m/s forward flight velocities. The intricate interplay between wing orientation, effective angle of attack and the ensuing lift and thrust generation are discussed. The results show that wing twist and fold alleviate negative lift and thrust in the upstroke, and in some cases producing persistent positive thrust throughout cycle for handwing. As a result, power consumption drops precipitously compared to the base case of a rigid flat plate. Another crucial realization is the relative importance of wing twist and fold in achieving efficient flight strongly depends on speeds. At slow flight, twist is significantly more effective in minimizing the power, but becomes energetically inefficient for fast speeds. The results also show that a 45° wing fold during upstroke is energetically beneficial for all speeds. The synergy of wing twist and fold are most prominent at slow flight. These findings provides useful guidelines for designing flapping wing robots.**

## I. Introduction

One of the challenges in designing a flapping wing robot is the trade off between system performance and wing complexity [1], [2], [3]. Studies show that highly-maneuverable bats easily control dozens of wing joints actuated by muscles and tendons [4], [5], [6] which renders superficial replication extremely difficult if not impossible. It is also likely that many of the wing degrees of freedom might not be relevant for flight performance, but rather dedicated to the animal's everyday activity, such as forage or mating [4], [5], [7]. Therefore, researchers gradually add complexity to the wing morphology and study the effect of the added degrees of freedom [8], [9], [6]. Wood et al. [8] used piezo-electric materials to directly drive the flapping motion of insect-inspired wings. They used a hinge flexure to limit the range of passive rotation with no direct control over twist motion, consistent with the relatively rigid insect wing. Numerically, Young et al. [10], used computational fluid dynamics (CFD) simulation, demonstrated that untwisted model of a desert locust is 15% less efficient in terms of power economy which defined as the ratio of time-averaged force to total power. Zheng et al. [11], also through CFD simulation of a Painted Lady butterfly (*Vanessa cardui*), found that wing twist is more important than camber in forward flight, in that by incorporating this feature, the simulated model recovers much of the performance of the observed wing kinematics. Phan et al. [12] used measured kinematics of a beetle-scale robot[13], through blade element theory, found the twist is especially effective in power-saving for high flapping frequency - up to 25% compared to flat-plate baseline. At a larger scale (birds or bats), capable of carrying substantial payload, He et al. [14] introduced a kestrel-sized flapping wing robot with one degree of freedom assigned to the flapping motion; the wing, made from kite cloth, deforms passively under aerodynamic loading. However, a prior experimental study by Wissa et al. [15] demonstrated that the passive wing deformation at this bird-scale can be inefficient, with a power consumption reaching $60-80$W for an operational flapping frequency of $4-6$Hz.

Send et al. [16] presented the "Smartbird" robot incorporating both wing twist and fold. They showed an impressive power consumption of 23W for 5m/s horizontal flight, which is only three to four times larger than the typical power consumption of birds with similar size and flight speed [17], [18]. However, in their design, the wing fold mechanism is fixed, and cannot adjust its amplitude to the flight speed, as what is observed in bats and bird flight [19], [20]. Moreover, in Send et al.'s robot, the wing twist motion is set as a constant angle - i.e., either a positive or negative angle of incident depending on the stroke - and is not synergisticly coupled to the flapping motion. This constraint prevents the robot from setting an optimal effective angle of attack, as is achieved by birds and bats [21], [22], [23]. More recently, Ramezani et al. [6] introduced a bat-inspired robot, "B2", with active wing retraction and wing twist, and demonstrated a promising flight capability. However, the wing twist is only actuated by the ventral-dorsal movement of the leg attached to the fuselage. This limits the range of pitch angle that can be realized, especially for the more flexible handwing [19], [22], [23]. In addition, the wing twist actuated in this way, tends to be larger at the wing root rather than the wing tip, which is opposite to what is observed in bat wing kinematics, especially during upstroke [22], [23]. Moreover, the wing fold is absent in Ramezani et al.'s design, which might not allow the proper orientation of the handwing to convert negative lift to beneficial thrust.

In this paper, we examine the effect of two important wing degrees of freedom (wing twist and fold in Fig. 1) on the performance of forward flight. We first develop a dynamical

[1]Center for Fluid Mechanics, School of Engineering, Brown University, Providence, RI, USA.e-mail: xiaozhou_fan@brown.edu
[2]Center for Fluid Mechanics, School of Engineering, Brown University, Providence, RI, USA.e-mail: kbreuer@brown.edu
[3]Mechanical, Robotics, and Industrial Engineering Department, Lawrence Technological University, Southfield, MI, USA. e-mail: hvejdanin@ltu.edu

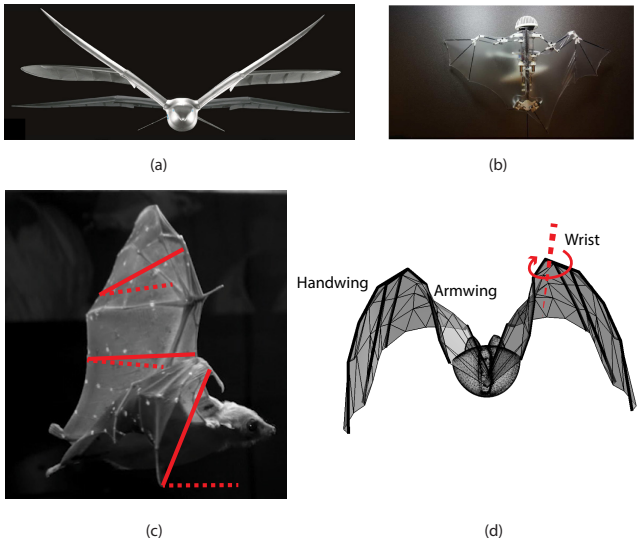


Fig. 1. Wing twist and fold found in design of flapping wing robot and animals. (a) Smartbird by Send et al. [16], notice the large wing fold and twist during uptroke. (b) Bat Bot by Ramezani et al. [6], the translucent membrane wing custom-made silicon skin. it can perform wing retraction-protraction and twist. (c) The live animal bat wing is seen to have different pitch angles along the span (wing twist), which is due to the active bending of digits in the handwing [23]. (d) For this 3D reconstructed bat wing model, during upstroke, the handwing would fold towards arwming, pivoting around the half-span wrist location.

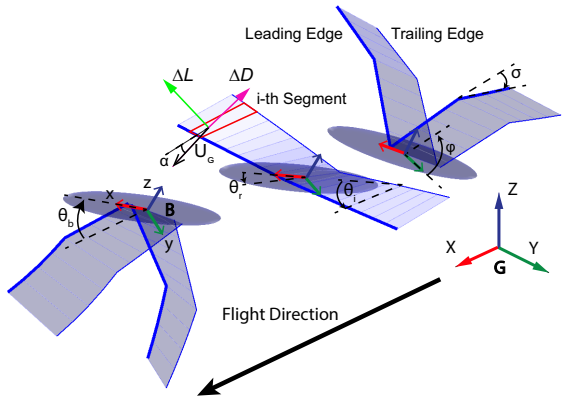


Fig. 2. Dynamic wing-body system with twist and folding capability. The wing mass is considered to be distributed along the armwing only. The folding motion ($\sigma$) is specified as a relative rotation between hand and armwing. The twist is defined as a linear distribution of increasing pitching angle from root ($\theta_r$) to tip ($\theta_i$, with indices $i =$ wing tip).

model that includes flapping, fold and twist motions for wings. Then through an optimization scheme, we find steady-state solutions for various forward speeds (2, 5 and 8 m/s) with minimized flapping frequency. The results first present the benefits of wing twist or fold separately, and then the synergistic benefit when they are combined. The cost of transport for different combinations of wing twist and fold is explored at the aforementioned flight speeds. Finally, we introduce an experimental platform that will be used in future work to validated these predictions.

## II. Methodology

### A. Wing and Body Kinematics

The two-wing, one body dynamical system is and extension of the work of Vejdani *et al.* [24], [25] and Parslew *et al.* [26], [20], and takes into account the wing twist and fold degrees of freedom observed in animal flight [27], [7], [28], [23].

Figure 2 shows the model in a global (**G**) and body-fixed (**B**) coordinate system. In the global coordinate system (**G**), $X$-axis is defined as forward direction, $Z$ as vertically-upward direction and $Y$ can be determined based on the right-hand rule. For the body coordinate system (**B**), the $x$-axis always points towards the head, $y$-axis points to the left side of the body and $z$ could thus be determined. For a forward flight considered in this paper, the body has two translational degrees of freedom $X_b$ and $Z_b$ in the longitudinal $X-Z$ plane, as well as pitch motion ($\theta_b$ in reaction to the aerodynamic torques. The generalized coordinate for the body in global coordinate, **G**, is thus given by $\mathbf{q}_b = [X_b, Z_b, \theta_b]^T$.

The wing kinematics are defined in the body-fixed coordinate system, **B**, (Fig. 2) where its $x$-axis points to the heading of the body, $y$-axis points towards the left of the body and $z$-axis directs the dorsal side of the body. In this coordinate, we assume the flapping and pitching angles, , $\phi_r, \theta_r$, at the wing root as:

$$\phi_r = -\Phi_r \cos(2\pi f t) \quad (1)$$

$$\theta_r = -\Theta_r \sin(2\pi f t + \Theta_p) + \Theta_o, \quad (2)$$

where $f$ is the flapping frequency, and $t$ is time. $\Phi_r, \Theta_r$ are the amplitudes of the wing root flapping and pitching motions respectively. $\Theta_p$ is the phase lag between flapping and pitching motion, and $\Theta_o$ is the offset angle for the pitching motion. Note that $\Theta_p$ and $\Theta_o$ are not defined *a prior*, but rather a result of the optimization scheme (see Vejdani et al. [24]). The wing twist simply means that each segment along the span has a different pitch angle, and in this study, we simplified the wing twist to be a linearly-varying pitch angle from the wing root to tip. Mathematically, for the $i$-th wing segment, its pitch angle $\theta_i$ is:

$$\theta_i = \theta_r \left( \frac{i-1}{N-1}(\xi - 1) + 1 \right), \quad (3)$$

where $\theta_r$ is the wing root segment pitch angle, $N$ is the total number of wing segments, and $\xi$ is the tip to root pitch angle ratio. For the wing fold, we assumed the axis of wing fold is exactly at the half-semispan, and that the folding is an additional rotation of the handwing with respect to the armwing; thus the time-varying relative rotation angle, $\sigma$, is defined as:

$$\sigma = -1/2\Sigma \sin(2\pi f t) + 1/2\Sigma, \quad (4)$$

where $\Sigma$ is the amplitude of the fold angle. A similar definition is used by Parslew *et al.* [26], [20].

### B. Aerodynamics

Blade element theory [29], [26] is used to model the aerodynamic forces. Specifically, the left and right wings are divided into $N = 10$ equal width segments (Fig. 2), with each segment approximating that of a 2D airfoil in quasi-steady state which generates a local lift and drag force vector. The total force is then a vector summation over the elemental forces on each segment in the global coordinate, $\mathbf{G}$. It is worth mentioning that the effective angle of attack (eAoA) seen by each wing segment is different due to the different velocities of each wing segment.

The aerodynamic coefficients used in the lift and drag model are assumed as follows [30], [26] :

$$C_l = 1.6\sin(2\alpha) \quad (5)$$

$$C_d = 1.135 - 1.05\cos(2\alpha), \quad (6)$$

where $C_l$ and $C_d$ are the lift and drag coefficients respectively used for each local wing segments, and $\alpha$ is the effective angle of attack. As illustrated in Fig. 2, the segment-wise lift, $\Delta L$, and drag, $\Delta D$, forces are then given as:

$$\Delta L = 1/2\rho C_l U_G^2 c\Delta r \quad (7)$$

$$\Delta D = 1/2\rho C_d U_G^2 c\Delta r, \quad (8)$$

where $\rho, c, \Delta r$ and $U_G$ are the air density, chord length, width, and airspeed of each segment in the global coordinate system, $\mathbf{G}$. The lift and drag on each segment are located at the quarter-chord.

### C. Equations of Motion

To construct the equations of motion, we assume the left and right wing motions to be symmetric, and therefore the dynamical model has 5 degrees of freedom in total. The wing fold and twist magnitude are parameters for the wing deformation, and that only the wing root kinematics, $\phi_r, \theta_r$ count as degrees of freedom. denoted by $\mathbf{q}_w = [\phi_r, \theta_r]^T$. Thus, we have $\mathbf{q} = [\mathbf{q}_b, \mathbf{q}_w]^T$ as the generalized degrees of freedom to use in the Lagrangian equation, and we construct the equations of motion as:

$$\mathbf{D}(\mathbf{q})\ddot{\mathbf{q}} + \mathbf{C}(\mathbf{q}, \dot{\mathbf{q}})\dot{\mathbf{q}} + \mathbf{g}(\mathbf{q}) = \tau + \mathbf{f}_{aero}, \quad (9)$$

where $\mathbf{D}, \mathbf{C}(\mathbf{q}, \dot{\mathbf{q}})$ and $\mathbf{g}(\mathbf{q})$ are the mass matrix, centrifugal matrix and gravitational vector respectively. The generalized torque, $\tau = [0_{1\times 3}, \tau_w]^T$ denotes the internal forces between the wing and the body, while $\mathbf{f}_{aero}$ represents the external aerodynamic forces and the ensuing torques felt by both left and right wings [24].

### D. Steady State Flight

A steady state flight is a solution of the equations of motion in which the following equations are satisfied:

$$[\mathbf{q}, \dot{\mathbf{q}}]_t = [\mathbf{q}, \dot{\mathbf{q}}]_{t+T} + \Delta \cdot T, \quad (10)$$

where $t$ is an arbitrary instant of time and $T$ is the wingbeat period. $\Delta$ is a 10-valued vector: $\Delta = [U_x, U_z, 0, 0, 0, 0, 0, 0, 0, 0]^T$, which accounts for the net displacement during flight. Here, $U_x$ and $U_z$ are the cycle-averaged velocity components along the forward ($X$) and vertical ($Z$) directions in the global coordinate system, $\mathbf{G}$, and are defined as inputs. If $U_x, U_z = 0$, this becomes the more familiar expression for hovering flight, while $U_z = 0$, represents straight-line level flight. Depending on the sign of $U_z$, the flight could be either descending or ascending. In this paper, we focus on the forward and level flight where $U_z = 0$. To find these limit cycles, we use the multiple shooting method [31], ensuring robust numerical convergence. Naturally, for a reasonable forward speed, $U_x$, there is a infinite set of possible wing kinematic parameters $(\Theta_p, \Theta_o, f)$ that satisfy the constraints (eq. 10), given appropriate initial conditions $(\mathbf{q}_0, \dot{\mathbf{q}}_0)$. Therefore, an overarching optimization scheme is built on top of the multiple shooting method which minimizes the flapping frequency, $f$. In other words, the optimization searches over all candidates of wing kinematics that result in the prescribed forward speed, $U_x$, and finds the one with minimum frequency, $f$. A typical periodic cycle for forward flight is given in Fig. 3.

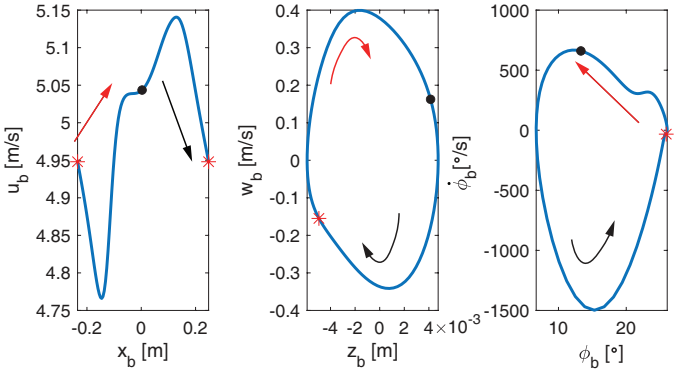


Fig. 3. A typical limit cycle of the body for a cycle averaged forward speed of 5 m/s. The red star and black dot indicate the begining of downstroke and upstroke respectively. The red and black arrow indicate time progression for downstroke and upstroke. $u_b, w_b$ and $\dot{\phi}_b$ are the velocity along $X, Z$ direction and the body angular velocity along $Y$ in $\mathbf{G}$.

### E. Dynamical and Morphological Parameters

We assume that the flapping wing robot shares similar dimensions, weight and morphological parameters of the medium-sized lesser-nosed dog-faced fruit bat, *Cynopterus brachyotis*[7], [32], [23] (Table. I). Animal measurements indicate that 80% - 90% of the wing mass is located in the armwing (for bats, see [28], Supplementary Table S2, and for birds, see[27]). Therefore, to simplify our model, we assume that only armwing has mass, distributed along the quarter-chord spanline.

### F. Power Expenditure and Cost of Transport

Once the steady state flight is obtained, and $\mathbf{q}$ and $\dot{\mathbf{q}}$ are known, we can calculate the cycle-averaged power and the cost of transport. Concretely, at time $t$, the instantaneous total power $P_{tot}$ is obtained as [25], [20]:

$$P_{tot}(t) = \tau_w \dot{\mathbf{q}}_w, \quad (11)$$

TABLE I

MORPHOLOGICAL PARAMETERS OF MODELED FLAPPING WING ROBOT

| | |
|---|---|
| Total Weight | 0.034 kg |
| Wings Weight | 0.006 kg |
| Wing Span | 0.36 m |
| Aspect Ratio | 6 |
| Body Pitch Moment of Inertia | $6 \cdot 10^{-6}$ kg m$^2$ |
| Wing Root Pitch amplitude,$\Theta_r$ | 15 deg. |
| Flapping amplitude,$\Phi_r$ | 45 deg. |

where $\dot{\mathbf{q}}_w$ carries the generalized velocities of the two wings and $\tau_w$ represents the internal forces between the wings and body [25], [33]. Any elastic energy stored in the membrane is assumed to be small and is neglected. Furthermore, only the positive power $P^+_{tot} = [P]^+_{tot}$ ($[.]^+$ is an operator that only accepts non-negative values) is considered in calculating the cycle-averaged power $\bar{P}_{tot}$ as:

$$\bar{P}_{tot} = 1/T \int_0^T P^+_{tot}\, dt \tag{12}$$

Finally, the non-dimensionalized cost of transport ($COT$) is defined as

$$COT = \bar{P}_{tot}/(mgU_x) \tag{13}$$

## III. RESULTS AND DISCUSSION

To understand how the twist and wing fold impact the aerodynamics and henceforth the cost of transport, we selected a medium flight speed, $U_x = 5$ m/s, to study in detail. We chose two segments at the $1/4$ and $3/4$ semi-span locations of the wing to represent the aerodynamics from arm- and handwing for the following discussion. All the forces (lift and thrust) presented are normalized by the weight of the model. It is noted that, since all the solutions presented below are periodic, it follows, by definition, that the cycle-averaged thrust is zero and that the lift is unity. For the base case, the twist ratio is $\xi = 1$ and fold amplitude is $\Sigma = 0^\circ$.

### A. The Aerodynamic Effect of the Wing Twist

Fig. 4 illustrates the effect of the wing twist on the aerodynamic forces. The results show that the optimization scheme finds a set of wing kinematic parameter $\Theta_p, \Theta_o$ that effectively eliminates the negative lift during upstroke. Because twist affects only the local pitch angle (thus altering the effective angle of attack), the force magnitude is relatively unchanged, but it is oriented to direct negative lift into a more positive thrust direction. This is especially true for the $3/4$ semi-span segment on the handwing, where the peak negative lift is reduced by half for the large twist case ($\xi = 3$), incurring only a small penalty (20%) in the maximum lift achieved during mid-downstroke. The inboard $1/4$ semi-span segment, representative of the armwing, sees a slight decrease in thrust for more twist, but in a much smaller scale compared to that gained by handwing. A similar trend of mitigating negative lift for the armwing is also observed, albeit to a lesser degree, due to a smaller effective velocity and pitch angle. It is clear that when twist is included, the peak forces reduce, which means that when one designs the drive mechanism for a vehicle, a smaller motor could be considered.

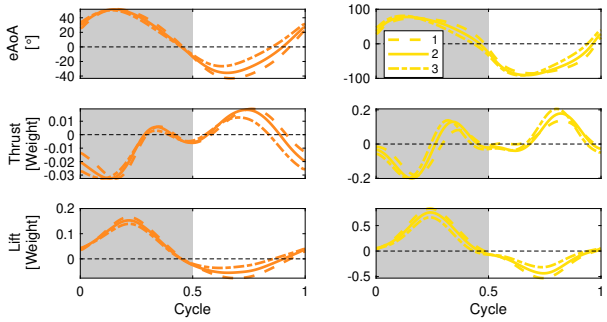


Fig. 4. Impact of twist alone on the aerodynamics at 5 m/s. The orange and gold color represent a segment in the armwing and handwing respectively. The dark shades indicate downstroke. The twist is specified as a spanwise linear pitch from the wing root to the wing tip, and the twist ratio $\xi$ is defined as the pitching amplitude ratio of wing tip to wing root. Three cases of twist ratio $\xi = 1, 2$ and 3 are considered here.

### B. The Aerodynamic Effect of the Wing Fold

Compared to the effect of twist on aerodynamics, the wing fold offers a distinctively different behavior when compared to the base case ($\xi = 1, \Sigma = 0^\circ$). The maximum fold angle of $\Sigma = 45^\circ, 90^\circ$ drastically changes the landscape of the effective angles of attack (eAoA) for both the arm- and handwing segments. Most notably, the eAoA for the armwing stays positive and around $20^\circ$ throughout the cycle; the handwing also has a much smaller negative eAoA peak, from $-100^\circ$ to $-30^\circ$ when $\Sigma = 45^\circ$, or $-45^\circ$ when $\Sigma = 90^\circ$. The reason for this is that the additional flapping motion of the handwing with respect to the armwing modifies the direction of the effective velocity of the handwing segment, especially during upstroke. As a result, although both the peak positive lift and thrust are reduced, the negative peaks are also reduced by an even greater extent. The armwing now produces positive lift throughout the cycle, while the handwing produces little negative lift during upstroke, as compared to the case of the wing without folding. The large drag observed for the handwing during downstroke also disappears. This suggests, as in the case for the wing twist, that a less powerful motor could be used when wing fold is incorporated.

The mitigation of negative lift and drag have two major impacts on the power expenditure (Fig. 6). First of all, because the cycle-averaged lift for forward and level flight is unity, and the thrust is exactly zero (thrust balances drag), the optimization no longer seeks a solution (wing kinematic parameters) that compensates the negative lift with a large positive ones. Secondly, the negative lift during the upstroke also demands power from the shoulder to sustain, which significantly increases the overall power consumption, and thus reduces the flight time for a flapping wing robot with a fixed energy source. Additionally, the instantaneous *peak* power requirement is reduced by the adoption of wing folding from 80W to 10W.

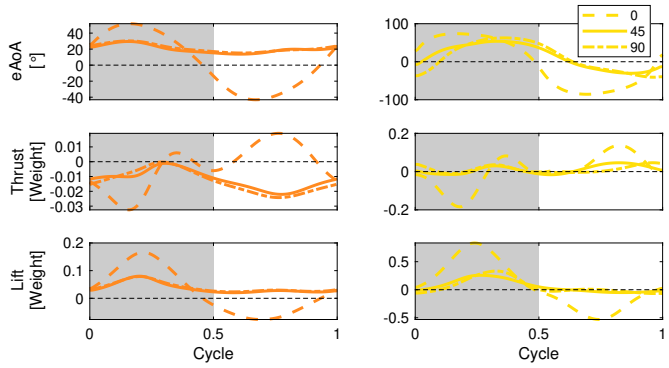


Fig. 5. Impact of fold alone on the aerodynamics at 5 m/s. The orange and gold color represent a segment in the armwing and handwing respectively. The dark shades indicate downstroke. We assumed the axis of wing fold is exactly at the half-semispan, and that the folding is an additional time-varying relative rotation (with amplitude being $\Sigma$) of the handwing with respect to the armwing. Here, three cases of increasing maximum folding angles $\Sigma = 0, 45$ and 90 are presented.

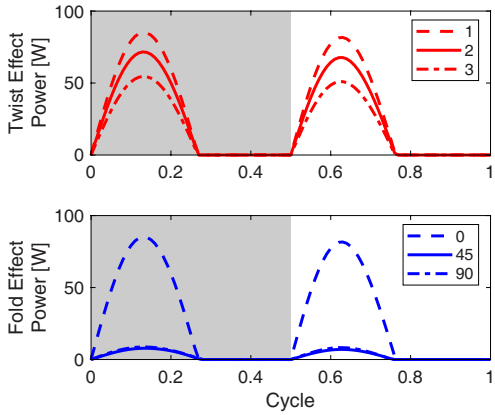


Fig. 6. Temporal energy expenditure of the flapping wing system at 5 m/s, for twist $\xi = 1, 2$ and 3, or fold $\Sigma = 0, 45$ or 90°. The darks shades indicate downstroke.

### C. Synergistic Effects of Wing Fold and Twist

Here, we look at the aerodynamic forces when wing fold and twist are combined. As seen in Fig. 7 for the flight speed of 5 m/s, when there is large fold angle ($\Sigma = 90°$), the handwing tends to generate larger peaks (positive and negative) in both thrust and lift, as compared to the case of moderate fold angles ($\Sigma = 45°$). When both twist and fold magnitudes are large ($\Sigma = 90°, \xi = 3$), the optimization finds a solution where the armwing lift force peaks during upstroke while the handwing lift peaks during downstroke. Therefore, with proper coordination of wing fold and twist, the required motor torque could be further reduced.

Fig. 8 shows the cost of transport for three flight speeds: 2, 5 and 8 m/s. Note that the definition of cost of transport (eq. 13) factors out the effect of speed, $U$. At low speed (2 m/s), the twist has a prominent impact on the COT, and a large twist ($\xi = 3$) with moderate amount of fold, $\Sigma = 45°$, achieves a minimum COT value. At a medium speed (5 m/s), the optimal COT for fold stays around $\Sigma = 45°$, and a

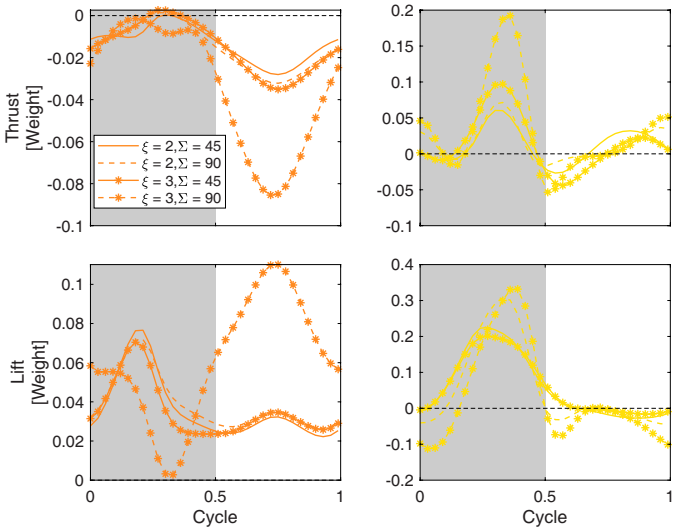


Fig. 7. Impact of fold and twist combined on the aerodynamics at 5 m/s. The orange and gold color represent a segment in the armwing and handwing respectively. The darks shades indicate downstroke.

medium-valued twist ($\xi = 2$) is needed. However, the COT gradient in this case is dominated by wing fold, and the COT is quite flat for $\Sigma > 40°$, indicating a large possible pool of kinematic choices in design. At high speed (8 m/s), the range of COT is much narrower than at low and medium speeds, and sensitive to both twist and fold. The most efficient way to fly in this scenario would still be with a fold of $\Sigma = 45°$ and without any twist. In summary, for the flight velocities studied, the results indicate that even a constant (including a passively designed mechanism) wing fold angle of $\sim 45°$ enhances the efficiency of the system, compatible with the results of Wissa et al. [15]. On the other hand, the effect of wing twist is more significant at lower speeds, suggesting the benefit of adjusting twist based on velocity. These optimal results reported here are also consistent with the Smartbird COT [16] at 5 m/s (reported around 1.1, predicted here 1.3). It should be noted that the predicted COT values in this paper consider the inertial and aerodynamic forces [25], but not the implementation for the entire system (e.g., driving mechanism) [34].

### D. Physical Model

To test the quasi-steady aerodynamics of the model current that that includes wing twist and fold, a two degrees-of-freedom physical model is proposed. As seen in Fig.9, a brushless motor generates the flapping motion through a 4-bar linkage, while a second servo motor can independently modulate the wing twist. There are torsional springs distributed along the main spar of the wing; the stiffness of these springs controls the twist of the wing when actuated by the servo motor. The wing fold is currently being implemented passively with a compliant joint, similar to Wissa et al. [15].

## IV. Conclusions

In this paper, we have incorporated the wing fold and twist into a previously-validated flapping wing dynamical model.

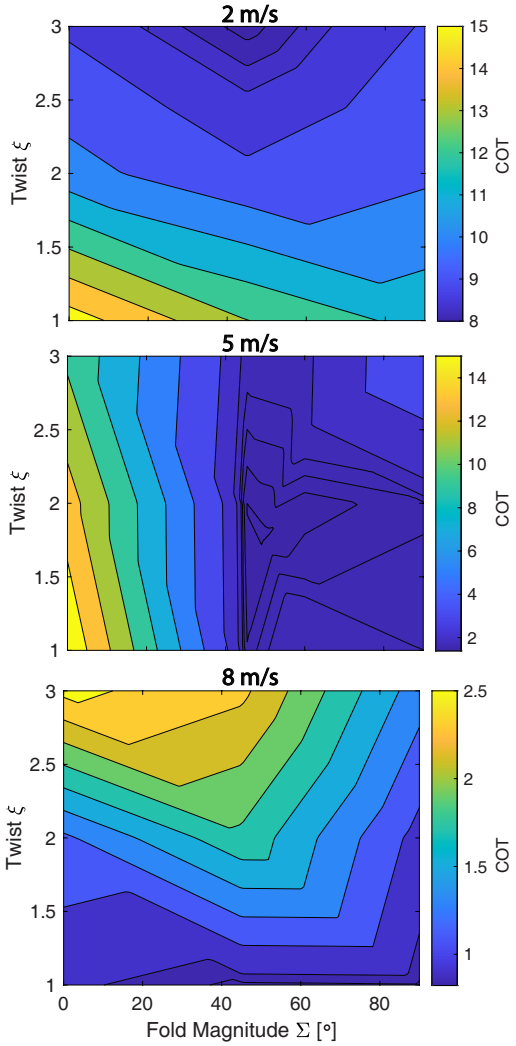


Fig. 8. The nondimensional cost of transport ( $P/(mgU)$ ) as a function of wing twist and fold magnitudes for three representative flight speeds typical for a flapping wing robot.

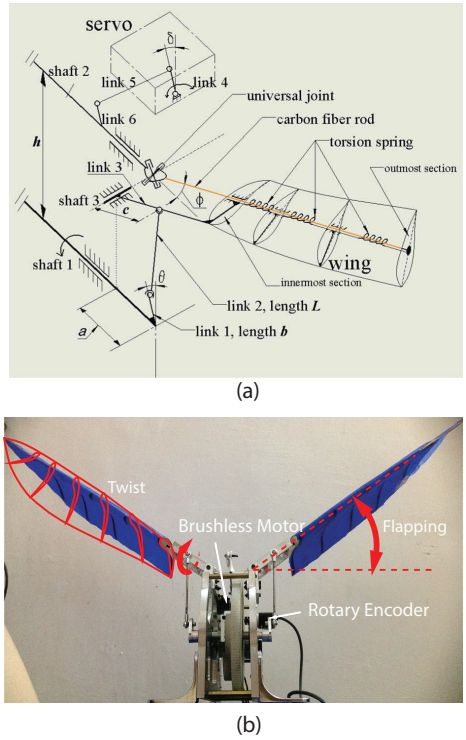


Fig. 9. Physical model to study the effect of twist. (a) Torsional spring were distributed along the spar for each wing segment and are controlled by the servo. (b) The frontal view of the 2-DoF flapping wing mechanism to be tested in a wind tunnel.

We explored the parameter space for energy optimal design of a flapping wing robot and have found that both wing fold and twist motions reduce the negative lift and thrust during upstroke and therefore, reduce the overall power consumption. For an optimal cost of transport robot design, a medium amount of fold in the upstroke (around $\Sigma = 45°$) seems to be beneficial across all flight speeds. These results support the idea of a passive implementation of the wing fold degree of freedom. The power advantage of the wing twist is more prominent at lower speeds, but has reduced benefit as the flight velocity increases.

## ACKNOWLEDGMENTS

This work is supported by the the China Scholarship Council (XF), Hyundai NGV (XF,KB) and National Science Foundation Grant 1931122 (HV).

## REFERENCES

[1] Wei Shyy, Hikaru Aono, Chang-kwon Kang, and Hao Liu. *An Introduction to Flapping Wing Aerodynamics*. Cambridge University Press, 2013.

[2] Wei Shyy, Chang-kwon Kang, Pakpong Chirarattananon, Sridhar Ravi, and Hao Liu. Aerodynamics, sensing and control of insect-scale flapping-wing flight. *Proceedings of the Royal Society A: Mathematical, Physical and Engineering Science*, 472(2186):20150712, 2016.

[3] Bo Cheng. Flying of Insects. *Bioinspired Structures and Design*, pages 271–299, 2020.

[4] U M Norberg. Functional osteology and myology of the wing of the dog-faced bat Roussettus aegyptiacus. *Z. Morph. Thiere*, 73(1):1–44, 1972.

[5] Joseph W Bahlman, Sharon M Swartz, and Kenneth S Breuer. Design and characterization of a multi-articulated robotic bat wing. *Bioinspiration {\&} Biomimetics*, 8(1):16009, 2013.

[6] Alireza Ramezani, Soon-Jo Chung, and Seth Hutchinson. A biomimetic robotic platform to study flight specializations of bats. *Science Robotics*, 2(3):eaal2505, 2017.

[7] Daniel K. Riskin, David J. Willis, Jose Iriarte-Diaz, Tyson L. Hedrick, Mykhaylo Kostandov, Jian Chen, David H. Laidlaw, Kenneth S. Breuer, and Sharon M. Swartz. Quantifying the complexity of bat wing kinematics. *Journal of Theoretical Biology*, 254(3):604–615, 2008.

[8] Robert J. Wood. The first takeoff of a biologically inspired at-scale robotic insect. *IEEE Transactions on Robotics*, 24(2):341–347, 2008.

[9] Jian Zhang, Fan Fei, Zhan Tu, and Xinyan Deng. Design optimization and system integration of robotic hummingbird. *Proceedings - IEEE International Conference on Robotics and Automation*, pages 5422–5428, 2017.

[10] J. Young, S. M. Walker, R. J. Bomphrey, G. K. Taylor, and A. L. R. Thomas. Details of Insect Wing Design and Deformation Enhance Aerodynamic Function and Flight Efficiency. *Science*, 325(5947):1549–1552, 2009.

[11] Lingxiao Zheng, Tyson L. Hedrick, and Rajat Mittal. Time-Varying Wing-Twist Improves Aerodynamic Efficiency of Forward Flight in Butterflies. *PLoS ONE*, 8(1):1–10, 2013.

[12] Hoang Vu Phan, Quang Tri Truong, and Hoon Cheol Park. An experimental comparative study of the efficiency of twisted and flat flapping wings during hovering flight. *Bioinspiration and Biomimetics*, 12(3), 2017.

[13] Hoang Vu Phan, Taesam Kang, and Hoon Cheol Park. Design and stable flight of a 21 g insect-like tailless flapping wing micro air vehicle with angular rates feedback control. *Bioinspiration & Biomimetics*, 2017.

[14] Guangping He, Tingting Su, Taoming Jia, Lei Zhao, and Quanliang Zhao. Dynamics Analysis and Control of a Bird Scale Underactuated Flapping-Wing Vehicle. *IEEE Transactions on Control Systems Technology*, 28(4):1233–1242, 2020.

[15] A. A. Wissa, Y. Tummala, J. E. Hubbard, and M. I. Frecker. Passively morphing ornithopter wings constructed using a novel compliant spine: Design and testing. *Smart Materials and Structures*, 21(9), 2012.

[16] Wolfgang Send, Markus Fischer, Kristof Jebens, Rainer Mugrauer, Agalya Nagarathinam, and Felix Scharstein. Artificial hinged-wing bird with active torsion and partially linear kinematics. *28th Congress of the International Council of the Aeronautical Sciences*, pages 23–28, 2012.

[17] Pennycuick. *Modelling the flying bird*. Academic Press, 2008.

[18] M. Klein Heerenbrink, L. C. Johansson, and A. Hedenström. Power of the wingbeat: Modelling the effects of flapping wings in vertebrate flight. *Proceedings of the Royal Society A: Mathematical, Physical and Engineering Sciences*, 471(2177), 2015.

[19] Tatjana Y Hubel, Nickolay I Hristov, Sharon M Swartz, and Kenneth S Breuer. Wake structure and kinematics in two insectivorous bats. *Philosophical Transactions of the Royal Society B: Biological Sciences*, 371(1704):20150385, 2016.

[20] Ben Parslew and Ben Parslew. Predicting power-optimal kinematics of avian wings. *Journal of the Royal Society Interface*, 12(102), 2015.

[21] Ben Parslew. *Simulating Avian Wingbeats and Wakes*. PhD thesis, The University of Manchester, 2012.

[22] Susheel Sekhar, Peter Windes, Xiaozhou Fan, and Danesh K. Tafti. Canonical description of wing kinematics and dynamics for a straight flying insectivorous bat (Hipposideros pratti). *PLoS ONE*, 14(6), 2018.

[23] Xiaozhou Fan and Kenneth Breuer. Reduced-order modeling of a bat flying with heavy and highly articulated wings. In *AIAA Bio-Inspired Aerodynamics II*, pages 1–14, 2021.

[24] Hamid Vejdani, David Boerma, Sharon M. Swartz, and Kenneth S. Breuer. Guidelines for the design and control of bio-inspired hovering robots. *Proceedings - IEEE International Conference on Robotics and Automation*, pages 4160–4166, 2017.

[25] Hamid R. Vejdani, David B. Boerma, Sharon M. Swartz, and Kenneth S. Breuer. The dynamics of hovering flight in hummingbirds, insects and bats with implications for aerial robotics. *Bioinspiration and Biomimetics*, 14(1), 2019.

[26] Ben Parslew and William J. Crowther. Simulating avian wingbeat kinematics. *Journal of Biomechanics*, 43(16):3191–3198, 2010.

[27] Tyson L. Hedrick, James R. Usherwood, and Andrew A. Biewener. Wing inertia and whole-body acceleration: An analysis of instantaneous aerodynamic force production in cockatiels (Nymphicus hollandicus) flying across a range of speeds. *Journal of Experimental Biology*, 207(10):1689–1702, 2004.

[28] Attila J Bergou, Sharon M Swartz, Hamid Vejdani, Daniel K Riskin, Lauren Reimnitz, Gabriel Taubin, and Kenneth S Breuer. Falling with Style: Bats Perform Complex Aerial Rotations by Adjusting Wing Inertia. *PLoS Biology*, 13(11):1–16, 2015.

[29] H. Glauert. *The Elements of Aerofoil and Airscrew Theory*. Cambridge University Press, 6 1983.

[30] James R. Usherwood. The aerodynamic forces and pressure distribution of a revolving pigeon wing. *Experiments in Fluids*, 46(5):991–1003, 2009.

[31] J Betts. *Practical Methods for Optimal Control and Estimation Using Nonlinear Programming*. Society for Industrial and Applied Mathematics, second edition, 2010.

[32] José Iriarte-Díaz, Daniel K Riskin, David J Willis, Kenneth S Breuer, and Sharon M Swartz. Whole-body kinematics of a fruit bat reveal the influence of wing inertia on body accelerations. *Journal of Experimental Biology*, 214(9):1546–1553, 2011.

[33] Gordon J. Berman and Z. Jane Wang. Energy-minimizing kinematics in hovering insect flight. *Journal of Fluid Mechanics*, 582:153–168, 2007.

[34] Zhan Tu, Fan Fei, Jian Zhang, and Xinyan Deng. An At-Scale Tailless Flapping-Wing Hummingbird and Experimental Validation. *IEEE Transactions on Robotics*, 36(5):1–15, 2020.